JACS
JOURNAL OF THE AMERICAN CHEMICAL SOCIETY

ARTICLE

pubs.acs.org/JACS

Intermediate-Assisted Multifunctional Catalysis in the Conversion of Flavin to 5,6-Dimethylbenzimidazole by BluB: A Density Functional Theory Study

Xiao-Lei Wang and Jun-Min Quan*

Laboratory of Chemical Genomics, School of Chemical Biology and Biotechnology, Peking University Shenzhen Graduate School, Shenzhen 518055, China

Supporting Information

ABSTRACT: BluB is a distinct flavin destructase that catalyzes a complex oxygen-dependent conversion of reduced flavin mononucleotide ($FMNH_2$) to form 5,6-dimethylbenzimidazole (DMB), the lower ligand of vitamin B_{12}. The catalyzed mechanism remains a challenge due to the discrepancy between the complexity of the conversion and the relative simplicity of the active site of BluB. In this study, we have explored the detailed conversion mechanism by using the hybrid density functional method B3LYP on an active site model of BluB consisting of 144 atoms. The results indicate that the conversion involves more than 14 sequential steps in two distinct stages. In the first stage, BluB catalyzes the incorporation of dioxygen, and the fragmentation of the isoalloxazine ring of $FMNH_2$ to form alloxan and the ribityl dimethylphenylenediimine (DMPDI); in the second stage, BluB exploits alloxan as a multifunctional cofactor, such as a proton donor, a proton acceptor, and a hydride acceptor, to catalyze the remaining no fewer than 10 steps of the reaction. The retro-aldol cleavage of the C1′−C2′ bond of DMPDI is the rate-determining step with a barrier of about 21.6 kcal/mol, which produces D-erythrose 4-phosphate (E4P) and the ring-closing precursor of DMB. The highly conserved residue Asp32 plays critical roles in multiple steps of the conversion by serving as a proton acceptor or a proton shuttle, and another conserved residue Ser167 plays its catalytic role mainly in the rate-determining step by stabilizing the protonated retro-aldol precursor. These results are consistent with the available experimental observations. More significantly, the novel intermediate-assisted mechanism not only provides significant insights into understanding the mechanism underlying the power of the simple BluB catalyzing the complex conversion of $FMNH_2$ to DMB, but also represents a new type of intermediate-assisted multifunctional catalysis in an enzymatic reaction.

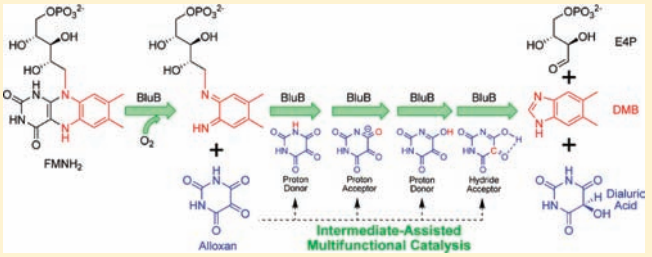

1. INTRODUCTION

Vitamin B_{12} is essential for human health; its deficiency results in pernicious anemia, neurologic injury, and hyperhomocysteinemia, and also is a risk factor for coronary heart disease and stroke.[1−5] The biological forms of vitamin B_{12} serve as crucial cofactors in diverse enzymes, such as the dehalogenases,[6,7] the isomerases,[8,9] and the methyltransferases.[10] The assembly of vitamin B_{12} requires more than 30 different enzymatic steps, which are now relatively well characterized.[11−14] However, the biosynthesis of 5,6-dimethylbenzimidazole (DMB), the lower axial ligand of vitamin B_{12}, was not well understood until recently. BluB has been identified as the essential enzyme that catalyzes the conversion of the reduced flavin mononucleotide ($FMNH_2$) to DMB.[15−17] The subsequently determined crystal structures of BluB by Walker et al.[18] provide further insights into understanding the mechanism of DMB formation, but the detailed mechanism of this remarkable reaction has not yet been fully established.

The conversion of $FMNH_2$ to DMB involves breaking three bonds and forming one bond (Scheme 1a). Previous studies have shown that DMB is synthesized from $FMNH_2$ through an oxygen-dependent manner,[19,20] and the C2 carbon of DMB is derived from the C1′ carbon of the ribose moiety of $FMNH_2$.[21] On the other hand, Begley et al.[22] reported that DMB could be formed from the ribose dimethylphenylenediamine (DMPDA) by a nonenzymatically oxidative cascade (Scheme 1b), which highlights that the ribose DMPDA might be an important intermediate in the formation of DMB. The ribityl side chain was converted to another product, D-erythrose 4-phosphate (E4P), in this process. Walker's recent work also confirmed the formation of E4P in the reaction catalyzed by BluB.[18] Despite these extensive studies, it is still unclear how the enzyme catalyzes the conversion of $FMNH_2$ to these products.

The crystal structure of BluB bound to $FMNH_2$ and molecular dioxygen provides a framework for understanding the roles of the dioxygen and enzyme in the reaction.[18] The dioxygen is anchored by two hydrogen bonds from the backbone amide of Gly61 and the O2′ hydroxyl group of $FMNH_2$ (the labeling of the atoms in this text are shown in Scheme 1a, $FMNH_2$), and is

Received: November 25, 2010
Published: February 23, 2011

dx.doi.org/10.1021/ja1106207 | J. Am. Chem. Soc. 2011, 133, 4079–4091

Scheme 1. (a) Conversion of $FMNH_2$ to DMB Catalyzed by BluB and (b) Formation of DMB via Nonenzymatic Oxidative Cascade

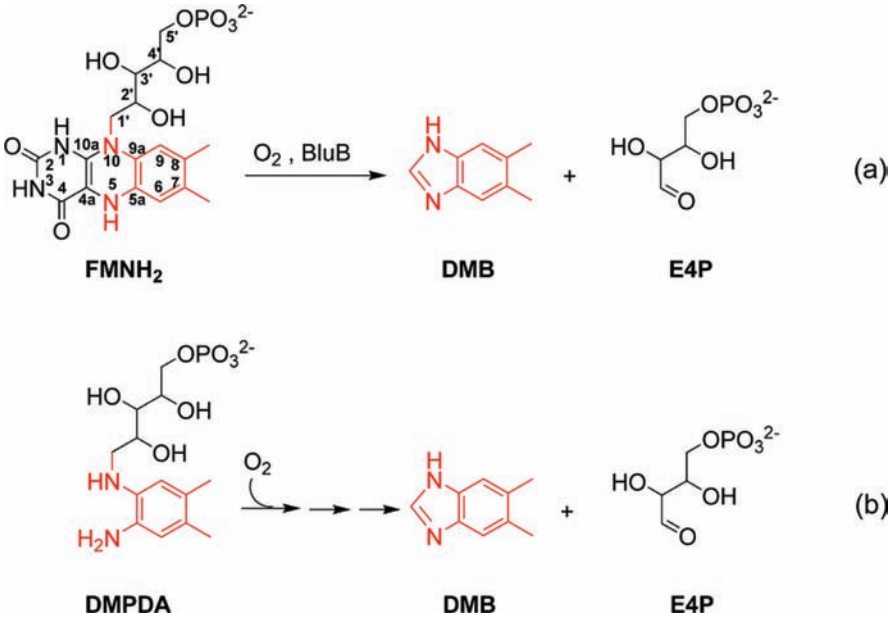

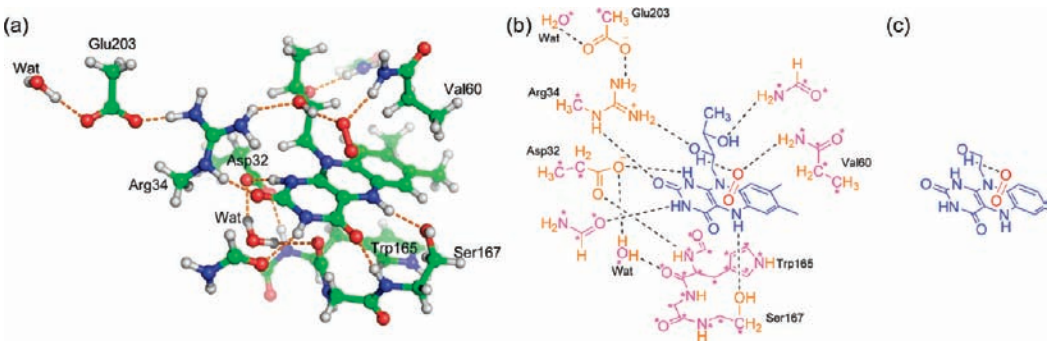

Figure 1. Active site model of BluB bound with $FMNH_2$ and O_2. (a) 3-D structure of the active site model. (b) Schematic representation of the active site model. Truncated $FMNH_2$ in blue, O_2 in red, flexible residues in yellow, constrained heavy atoms in purple and labeled with asterisk. (c) Schematic representation of the simple model.

well poised in the active site for attack at C4a to form the possible peroxyflavin intermediate. The two hydrogen bonds serve as a "peroxyanion hole" to facilitate this process. The isoalloxazine ring of $FMNH_2$ is fixed in the active site by the side chains and backbone amide of several conserved residues such as Asp32, Arg34, and Ser167.[15] Further biochemical studies showed the catalytic roles of Asp32 and Ser167, reflected by the fact that the mutations of Asp32Asn or Ser167Gly impede the formation of DMB. On the basis of the structural analysis, Walker et al. proposed two possible mechanisms for the catalysis,[18] but both of the mechanisms involve some uncommon reactions, such as the deprotonation of the unactivated C−H by the common amino acid Asp32, and the proton of the hydroxyl group serving as the hydride for the reduction. In addition, the sharp contrast between the relative simplicity of the active site of BluB and the complexity of the reaction also remains a significant challenge for the detailed catalytic mechanism of BluB.[18,23,24]

In this report, we applied density functional theory (DFT) to study the full reaction pathway of the conversion of $FMNH_2$ to DMB catalyzed by BluB, and demonstrated that the simple active site of BluB can catalyze all the steps of the conversion of $FMNH_2$ to DMB. We hope our results provide some insights into understanding the complex reaction catalyzed by BluB.

2. COMPUTATIONAL DETAILS

The active site model was derived from the crystal structure of BluB bound to $FMNH_2$ and molecular dioxygen (PDB code: 2ISL).[18] The model consists of a truncated $FMNH_2$, the bound dioxygen, and the interacting residues, Asp32, Arg34, Pro58, Ser59, Val60, Gly61, Leu108, Glu109, Gly164, Trp165, Val166, Ser167, and Glu203. Considering the balance between the computational efficiency and the protein environment, those residues were modeled by the truncated side chains or the backbone amide groups by taking into account the detailed interactions between $FMNH_2$ and BluB. Two crystallographic water molecules were also included to stabilize the charged residues in the gas phase. The established model consists of 144 atoms, with details shown in Figure 1. To evaluate the function of the residues in the active site, a simple model that only consists of substrates including the truncated $FMNH_2$ and O_2 was also studied.

dx.doi.org/10.1021/ja1106207 |J. Am. Chem. Soc. 2011, 133, 4079–4091

Scheme 2. Proposed Mechanism of BluB

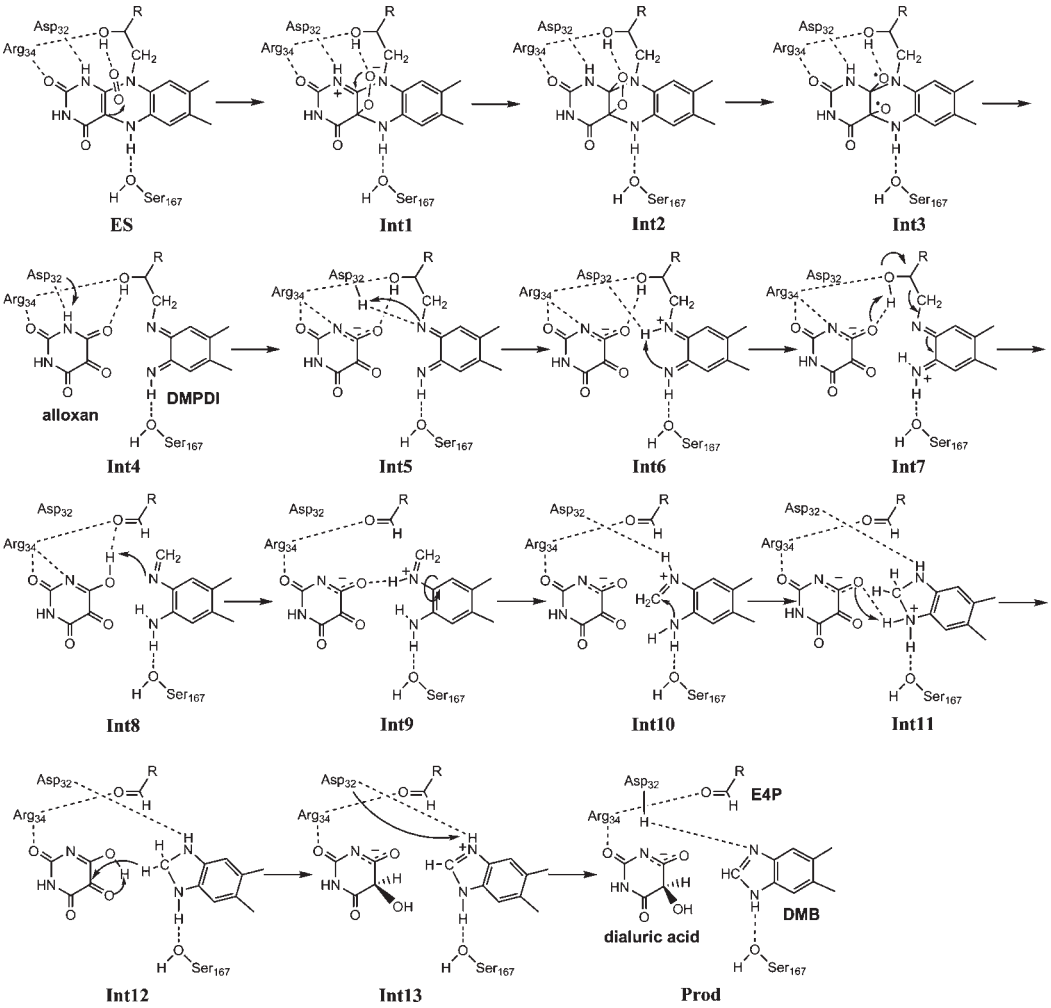

All the calculations were performed using density functional theory (DFT) as implemented in the Gaussian03 program.[25] The geometries of complex, intermediates, transition states, and product were optimized by using B3LYP/6-31G(d) level.[26,27] The single point electronic energies of the stationary points were calculated by using B3LYP/6-311+G** based on the B3LYP/6-31G(d) optimized structures. B3LYP has been widely used to study the reaction mechanisms of enzymes,[28−30] with an average error of 3 kcal/mol for molecules containing first- and second-row atoms.[31] This error is expected to be larger for the large systems with significant van der Waals interactions, but this error might not make the calculations unreliable since the potential energy surface is calculated by the relative energies of the stationary points rather than the absolute energies of them. Open shell systems were treated using unrestricted B3LYP (UB3LYP). The optimization of the singlet diradical species using the broken symmetry approach would cause a large spin contamination. Therefore, we used spin projection (SP) techniques to ensure a proper description of the singlet diradical species, as shown in eqs 1 and 2, where ${}^{X}E$ is the electronic energy and ${}^{X}\langle S^2\rangle$ is the total angular momentum of the spin state X.[32]

$$ {}^{\text{singlet}}E_{\text{SP}} = {}^{\text{singlet}}E + c_{\text{SC}}[{}^{\text{singlet}}E - {}^{\text{triplet}}E] \quad (1) $$

$$ C_{\text{SC}} = \frac{{}^{\text{singlet}}\langle S^2\rangle}{{}^{\text{triplet}}\langle S^2\rangle - {}^{\text{singlet}}\langle S^2\rangle} \quad (2) $$

During geometry optimization, some atoms were constrained at the initial positions in the crystal structure to maintain a reasonable geometry of the active site like that in the crystal structure and avoid the explosion of the active site (Figure 1b). All other degrees of freedom were optimized. The transition states were confirmed to have only one imaginary frequency along the reaction coordinates. Because some atoms in the model are constrained during optimization, all the optimized structures are not strictly stationary points; zero-point vibrational energy corrections and thermal effects are not sufficiently accurate and therefore not considered in this study.

The dielectric effects from the protein environment were calculated using the conductor-like polarizable continuum model (CPCM),[33] with the united atom Kohn−Sham topological model (UAKS)[34] for the atomic radii. The dielectric constant was set equal to 4.0 to mimic the protein environment.[35]

The minimum energy crossing point (MECP) between the triplet and singlet surfaces was located at the B3LYP/6-31G(d) level employing the methodology developed by Harvey et al.[36] Spin−orbital coupling (SOC) at the MECP was calculated with GAMESS package[37] by using the full Breit−Pauli operator.[38] To reduce the computational demand, a truncated structure of MECP that includes the truncated $FMNH_2$, the bound dioxygen, and the interacting Asp32 and Val60 was used for SOC calculations, and the singlet/triplet state-averaged complete-active-space self-consistent field CASSCF(4,3) wave function was used to approximately evaluate the SOC matrix elements. The triplet-singlet transition probability (P) was estimated by

dx.doi.org/10.1021/ja1106207 |J. Am. Chem. Soc. 2011, 133, 4079–4091

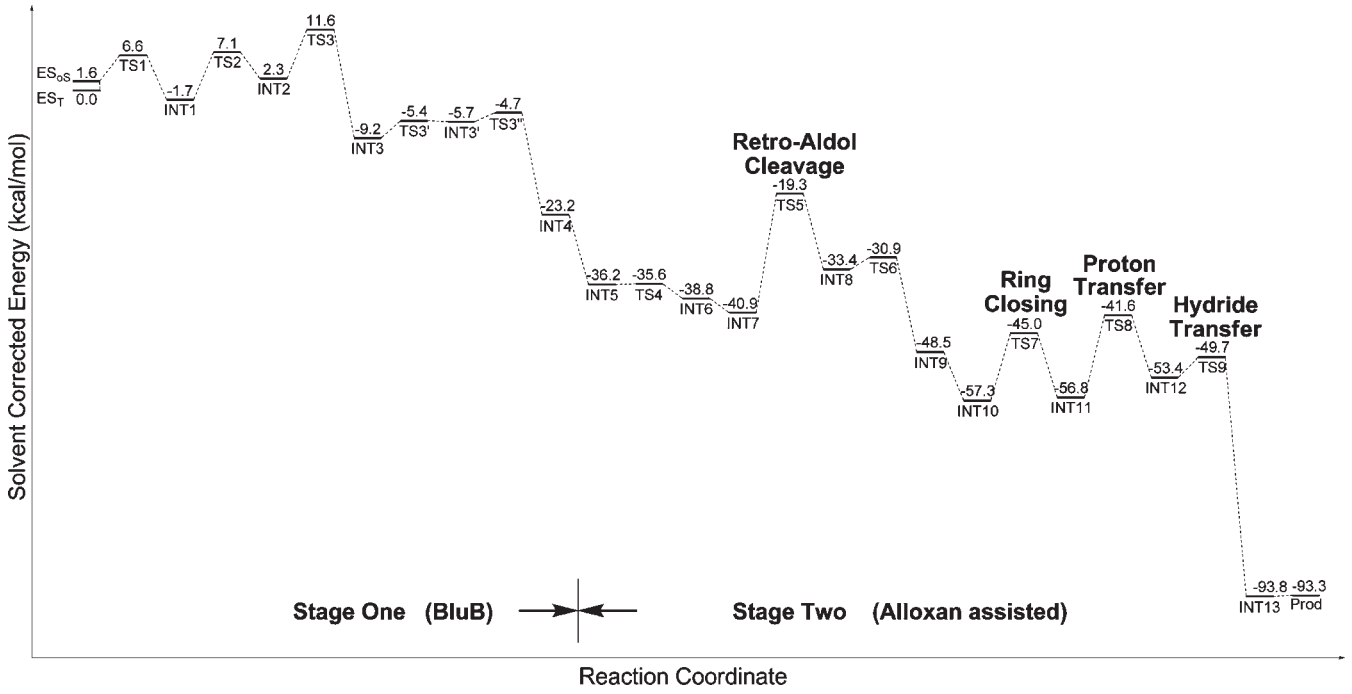

Figure 2. Calculated energy profile along the proposed reaction pathway for BluB. The pathway is separated into two stages based on whether alloxan is involved in the catalysis.

Landau−Zener formula[39]

$$P = 1 - \exp\left(\frac{-4\pi^2|H_{SOC}|^2}{h\nu|\Delta g|}\right)$$

where H_{SOC} is the SOC matrix element between the electronic states, and ν is the velocity with which the system is passing the crossing region, which has an upper bound of 418 ms^{-1} estimated from the kinetic theory of gases. Δg is the difference of the gradients calculated for the two states at the crossing point.

3. RESULTS AND DISCUSSION

The calculations suggest that the conversion of $FMNH_2$ to DMB proceeds via more than 14 steps in two distinct stages (Scheme 2 and Figure 2). The first stage is mainly catalyzed by BluB itself, including the activation of dioxygen, the formation of the dioxetane-like intermediate between the dioxygen and $FMNH_2$, and the breakdown of the dioxetane-like intermediate to form alloxan and the ribityl dimethylphenylenediimine (DMPDI). The second stage is catalyzed by the collaboration of BluB and alloxan, including the retro-aldol cleavage of the C1′−C2′ bond of DMPDI to form the D-erythrose 4-phosphate (E4P) and the ring closure precursor of DMB, the ring closing of the precursor, and the subsequent proton and hydride transfers to form the final product DMB.

3.1. ES Complex and Dioxygen Activation. The dioxygen molecule in the active site is anchored by two hydrogen bonds from the backbone amide of Gly61 and the O2′ hydroxyl group of $FMNH_2$, and well poised for attack at C4a. However, the dioxygen molecule has a triplet ground state, and its attachment to the closed shell singlet $FMNH_2$ to form a singlet peroxyflavin intermediate is a spin-forbidden process.[40,41] The reductive activation mechanism of triplet dioxygen has been well characterized in glucose oxidase by Siegbahn et al.[42,43] The initial step is a single electron transfer from the reduced $FADH_2$ to dioxygen to generate a triplet diradical pair ($FADH_2^{\bullet+}\cdots O_2^{\bullet-}$). This process is facilitated by the protonated His516 that activates dioxygen as a better electron acceptor. Once the superoxide-like species is formed, the stronger spin−orbit coupling (SOC) in the superoxide-like species increases significantly the probability of the triplet to singlet spin flip, leads to the open shell diradical pair ($FADH_2^{\bullet+}\cdots O_2^{\bullet-}$), and then forms the final closed shell singlet peroxyflavin intermediate. Given the similarity of the active site between BluB and glucose oxidase, the activation of the dioxygen by BluB should have a similar mechanism compared to that of glucose oxidase.

As shown in Figure 3, the backbone amide of Gly61 and the O2′ hydroxyl group of $FMNH_2$ that anchor dioxygen play a similar role to that of His516 in glucose oxidase to activate the dioxygen as a better electron acceptor. In addition, Asp32 partially deprotonates the N1 atom of $FMNH_2$ rendering $FMNH_2$ as a better electron donor. The catalytic role of Asp32 in the electron transfer process is consistent with the experimental observation that Asp32Ala or Asp32Asn mutants have significantly lower activity. The interacting network in the active site of BluB elegantly facilitates the electron transfer from $FMNH_2$ to dioxygen, as reflected by the significant decrease of the energy gap between the triplet ground state and the open shell singlet state (Figure 3).

The optimized structure of the triplet ES complex ($\mathbf{ES_T}$) indicates that dioxygen has obvious superoxide-like characteristics, manifested by the longer O−O bond distance (1.28 vs 1.21 Å in nonactivated dioxygen) and increased Mulliken charge on dioxygen. The optimized geometry of the open shell singlet state of ES complex ($\mathbf{ES_{oS}}$) is similar to that of the triplet ground state ($\mathbf{ES_T}$), and the distance between the C4a carbon of $FMNH_2$ and the O1 atom of dioxygen is about 2.65 Å, much shorter than that in the simple model (3.20 Å), which makes it easy for dioxygen attacking at C4a of $FMNH_2$ to form the peroxyflavin intermediate. Furthermore, opposite spins on dioxygen and C4a carbon

dx.doi.org/10.1021/ja1106207 |J. Am. Chem. Soc. 2011, 133, 4079–4091

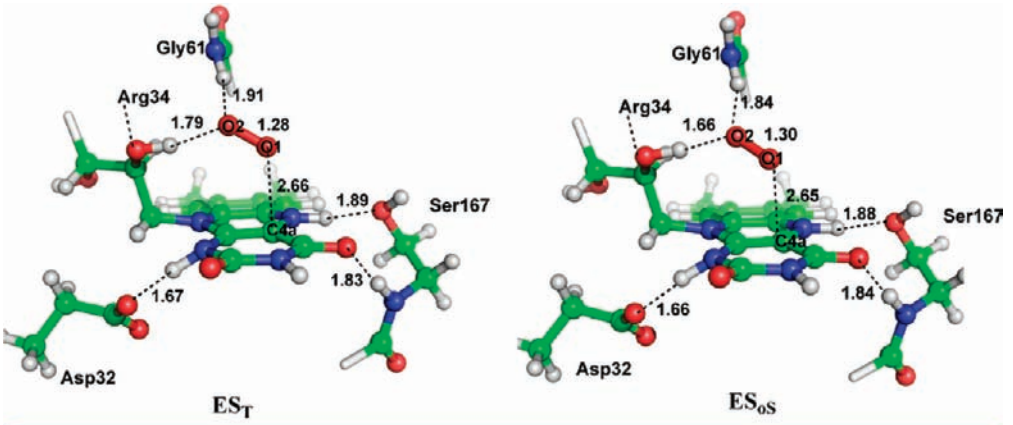

	O_2 (isolated)	O_2 (sM$_T$)	O_2 (ES$_T$)	O_2 (ES$_{oS}$)
$d_{O\text{-}O}$(Å)	1.21	1.23	1.28	1.30
$q_{O\text{-}O}$(e)	0.0	-0.114	-0.402	-0.553
$\Delta E_{T\text{-}S}$(kcal/mol)	20.6	14.1	1.6	--

Figure 3. Optimized structure of enzyme−substrate complex. Some residues are omitted for clarity. sM and ES represent the simple model and the enzyme−substrate complex model, respectively. The subscripts T and oS represent triplet state and open-shell singlet state, respectively. d_{O-O} is the distance between the two oxygen atoms of O_2, and q_{O-O} is the total Mulliken charge on them. $\Delta E_{T\text{-}S}$ represents the energy difference between the triplet state and the open shell singlet state. Hydrogen bonds are shown in dashed lines, and the distances are in angstroms.

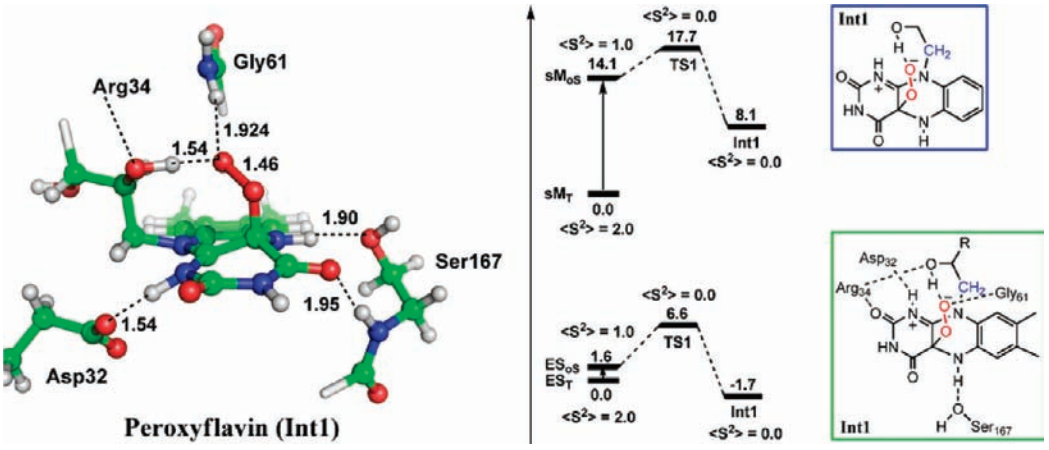

Figure 4. Optimized structure of peroxyflavin intermediate (**Int1**), and the energy profiles of the formation of **Int1** in two models. Some residues are omitted for clarity. sM and ES represent the simple model and the enzyme−substrate complex model, respectively. The subscripts T and oS represent triplet state and open-shell singlet state, respectively. Hydrogen bonds are shown in dashed lines, the distances are in angstroms, and energies are in kcal/mol.

also facilitate the bond formation between O1 of dioxygen and C4a (Figure S1).

3.2. Formation of Peroxyflavin Intermediate. As shown in Figure 4, the activation energy of forming the peroxyflavin intermediate (**Int1**) from the open shell singlet ES complex (**ES$_{oS}$**) is 5.0 kcal/mol, totally 6.6 kcal/mol from the triplet ground state **ES$_T$**. The newly formed peroxy anion is stabilized by the two hydrogen bonds from the backbone amide of Gly61 and the O2′ hydroxyl group of $FMNH_2$, and the positively charged imine N1 of **Int1** is stabilized by Asp32. On the other hand, the activation energy of forming the peroxyflavin anion from the triplet ground state in the simple model is about 17.7 kcal/mol, 11.1 kcal/mol higher than that in the active site model (Figure 4 and Figure S2). Since both the simple model and active site model have a similar hydrogen bond between the O2′ hydroxyl group of $FMNH_2$ and peroxy anion, the significant decrease of the activation energy in the active site model highlights the catalytic role of the active site residues, especially the highly conserved Asp32.

A spin transition must occur from the triplet ground state to the singlet **TS1** and **Int1**, and the MECP is the most favorable point for the spin crossing. The MECP was located at the C4a−O1 bond distance of 2.60 Å and about 3.3 kcal/mol higher than the triplet ground state, which is energetically close to the open-shell singlet state (Figure S3). The estimated H_{SOC} at the MECP is 96.1 cm^{-1}, in addition to the small difference of gradients (Δg = 3.4 kcal/mol/Å), which results in efficient spin transition

dx.doi.org/10.1021/ja1106207 |J. Am. Chem. Soc. 2011, 133, 4079–4091

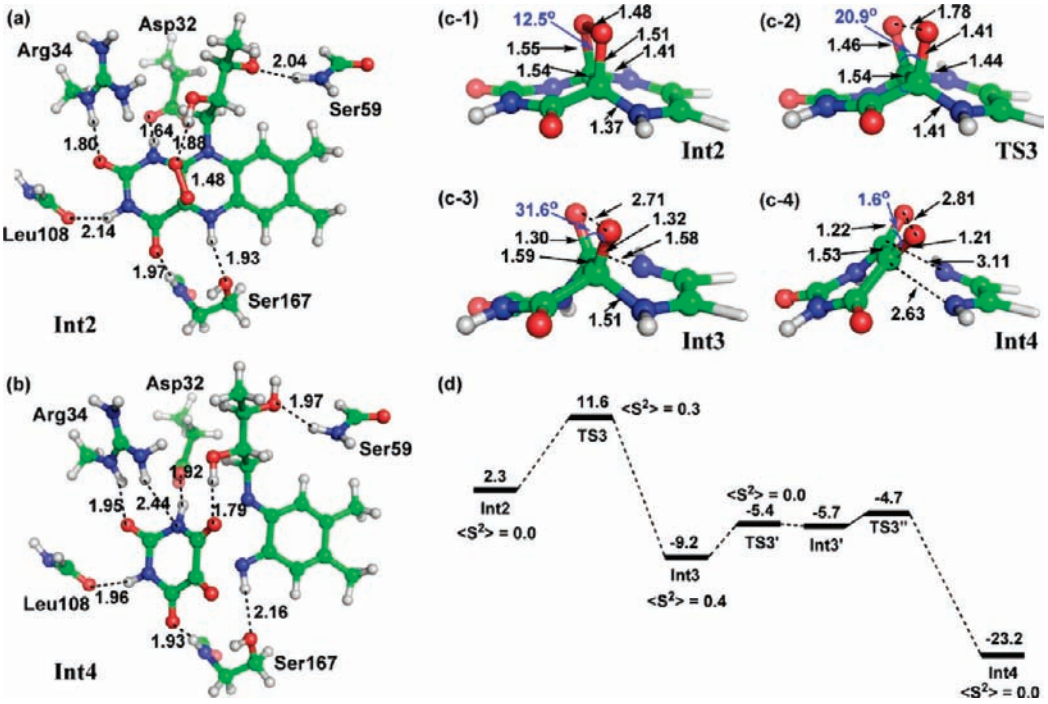

Figure 5. Optimized structures of dioxetane-like intermediate (a, c-1, **Int2**), ring-opening transition state (c-2, **TS3**), ring-opening intermediates (c-3, **Int3**; b, c-4, **Int4**), and the energy profile from **Int2** to **Int4**. Some residues and fragments are omitted for clarity. Hydrogen bonds are shown in dashed lines, the distances are in angstroms, and dihedral angles are in degrees.

($P = 0.89$) between the triplet state to the singlet state during the nucleophilic addition of dioxygen to C4a of $FMNH_2$. We should note that the geometry and properties of minimum-energy crossing points are sensitive to the calculational methods and the presence of solvent: the results presented here are therefore more qualitative rather than quantitative. However, even if the real crossing probability were 2 order of magnitude smaller ($P = 0.0089$) than the estimated crossing probability, the avoided crossing increases the barrier of transition by less than 3 kcal/mol, which has no significant influence on the potential surface as shown in Figure 2.

3.3. Formation of Dioxetane and O−O Bond Cleavage. The negatively charged peroxy anion and the highly polarized C10a carbon of the isoalloxazine ring in the peroxyflavin intermediate (**Int1**) facilitate the bond formation between O2 of peroxy anion and C10a carbon of isoalloxazine. This step proceeds over a barrier of 8.8 kcal/mol to form the dioxetane-like intermediate **Int2** (Figure 5 and Figure S4). It has been also observed that the flavin C4a-peroxide acts as a nucleophile attacking the substrates in other systems such as Baeyer−Villiger monooxygenase,[44−47] and bacterial luciferase,[48−50] but herein the substrate is the flavin itself. This self-attacking mechanism underlies the cannibalization of flavin by BluB. The dioxetane-like intermediate is not uncommon in reactions catalyzed by enzymes, and has been extensively studied in the reaction catalyzed by the firefly luciferase,[51−53] in which a highly energetic dioxetanone intermediate is formed and decomposes to the product. The decomposition mechanism of the dioxetane-like intermediate has been well characterized in the simplest 1,2-dioxetane and its more complex derivatives,[54−57] involving a singlet diradical transition structure with the O−O bond cleavage.

According to the similar mechanism, the dioxetane-like intermediate **Int2** and the ring-opening transition structure **TS3** were calculated by UB3LYP/6-31G(d) (Figure 5 and Figure S5). The calculated activation energy barrier from **Int2** to **TS3** is about 9.3 kcal/mol, which is relatively lower than that of the 1,2-dioxetane predicted by CASSCF/MP2 (about 16 kcal/mol),[57] and also lower than that of the decomposition of the dioxetanone derivative of the thiazole fragment of an oxyluciferin predicted with B3LYP/6-31G* (about 18 kcal/mol).[51] The lowering of the activation energy might be attributed to the stabilization of the radical by the aromatic ring system, which is shown in the following discussion.

The ring-opening transition structure **TS3** shows modest singlet diradical character with an $\langle S^2 \rangle$ value equal to 0.3, but we do not exclude the possibility that UB3LYP underestimates the diradical character.[57] **TS3** has an O1−O2 bond distance of 1.78 Å and elongated bond distances for C4a−N5 and C10a−N10, but the C4a−C10 bond distance does not change. The spin population analysis shows that part of the spin density is located on the two bond breaking oxygen atoms, and another part is spanned on the benzene diamine fragment and stabilized by the aromatic ring (Figure S5). The following **Int3** also has a similar singlet diradical character with O−O bond distance of 2.71 Å and C10a−N10 bond distance of 1.58 Å. Followed by two low barrier bond breakages for C4a−N5 and C10a−N10 bonds, the tricyclic flavin is separated into two fragments, alloxan and the ribityl dimethylphenylenediimine (DMPDI) (**Int4**). The fragmentation reaction is strongly exothermic by about 23.2 kcal/mol, which drives the reaction to be irreversible.

3.4. Retro-Aldol Reaction and Formation of E4P. As described above, the fragmentation of ribose flavin forms two species: alloxan and the ribityl dimethylphenylenediimine (DMPDI) (**Int4**). DMPDI has been proposed to be a critical intermediate for the nonenzymatic conversion of the ribose dimethylphenylenediamine (DMPDA) to DMB,[22] but the

dx.doi.org/10.1021/ja1106207 |J. Am. Chem. Soc. 2011, 133, 4079–4091

Scheme 3. Retro-Aldol Reaction of the Ribityl Dimethylphenylenediimine (DMPDI)

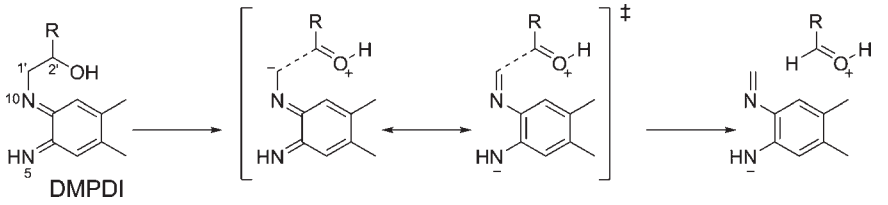

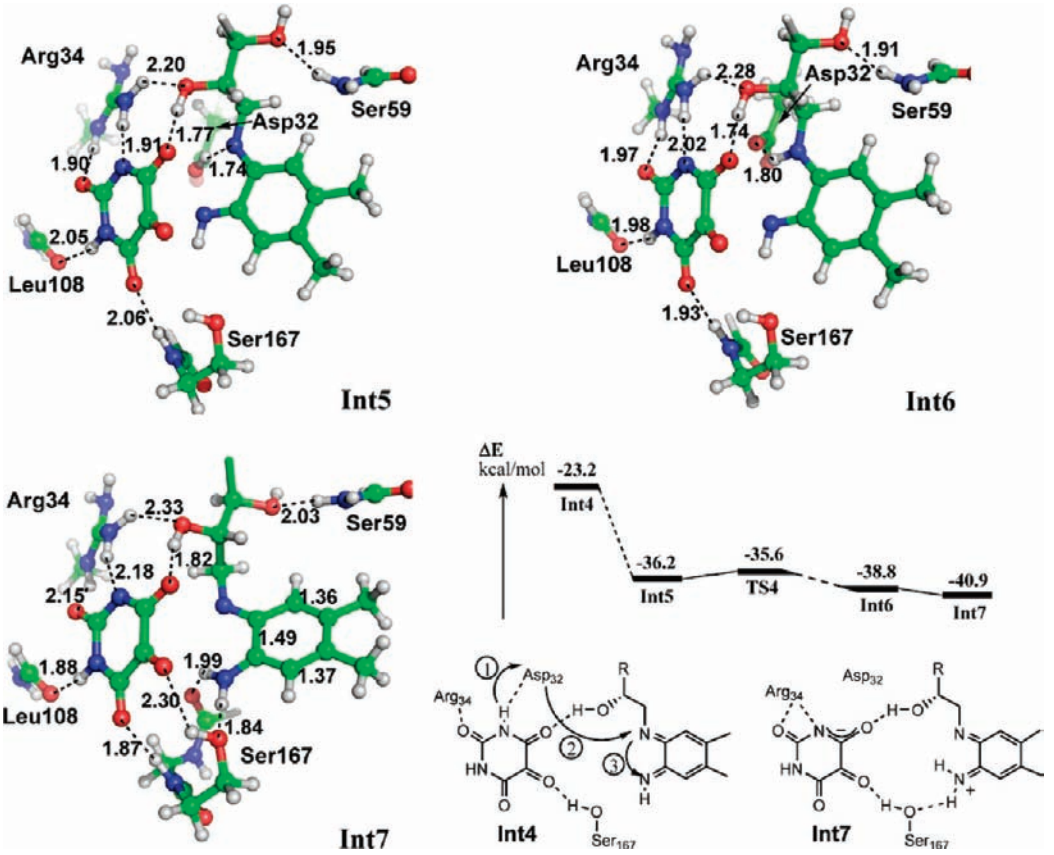

Figure 6. Optimized structures and energy profile of proton transfer intermediate (**Int5**−7). Some residues and fragments are omitted for clarity. Hydrogen bonds are shown by dashed lines, and the distances are in angstroms. The arrows in the schematic structure of **Int4** indicate the proton transfer direction from N1 to N5.

proposed cyclization of the diimine to form the ribose 2H-benzimidazole intermediate might be unfeasible in the active site of BluB due to the geometric constraint of the long ribityl side chain. Begley et al. also proposed a minor pathway in which a retro-aldol reaction occurs prior to the cyclization. However, to facilitate the retro-aldol reaction, there should be a base to deprotonate the hydroxyl group on C2′ carbon and a proton to neutralize the forming negative charge on N5 (Scheme 3). Our calculations indicate that the active site of BluB and the alloxan fragment produced in the previous step cooperatively facilitate the retro-aldol reaction.

As shown in Figure 5b, the N1−H bond of alloxan is highly polarized by both Asp32 and Arg34, which facilitates the proton transfer from N1 to the carboxylate side chain of Asp32. After the proton transfer, the newly formed negatively charged N1 is stabilized by Arg34, and the neutral carboxylate side chain of Asp32 forms another hydrogen bond with N10 of the diimine fragment (Figure 6, **Int5**), which makes **Int5** about 13.0 kcal/mol more stable than **Int4**. Meanwhile, the proton transfer from Asp32 to N10 occurs readily with a modest activation barrier (∼0.6 kcal/mol) and a slight energy gain (∼2.6 kcal/mol) (Figure 6, **Int6**). The proton is more favorably located on N5 rather than on N10 by about 2.1 kcal/mol, where the protonated N5 is stabilized by the backbone carbonyl oxygen of Trp165 and the side chain hydroxyl group of Ser167 (Figure 6, **Int7**). Detailed Mulliken charge analysis indicates that the negative charge on N1 of alloxan is partially spanned on the carbonyl oxygen O10a (−0.512 in **Int4** vs −0.587 in **Int7**), which would facilitate the proton transfer from the O2′−H group to O10a of alloxan in the subsequent retro-aldol cleavage. (Note: O10a is previously labeled as the oxygen O2 of dioxygen, and hereafter for clarity, it is labeled as O10a according to the connected C10a.)

As discussed above, both the deprotonation of N1 and protonation of N5 facilitate the retro-aldol reaction. The partially

dx.doi.org/10.1021/ja1106207 |*J. Am. Chem. Soc.* 2011, 133, 4079–4091

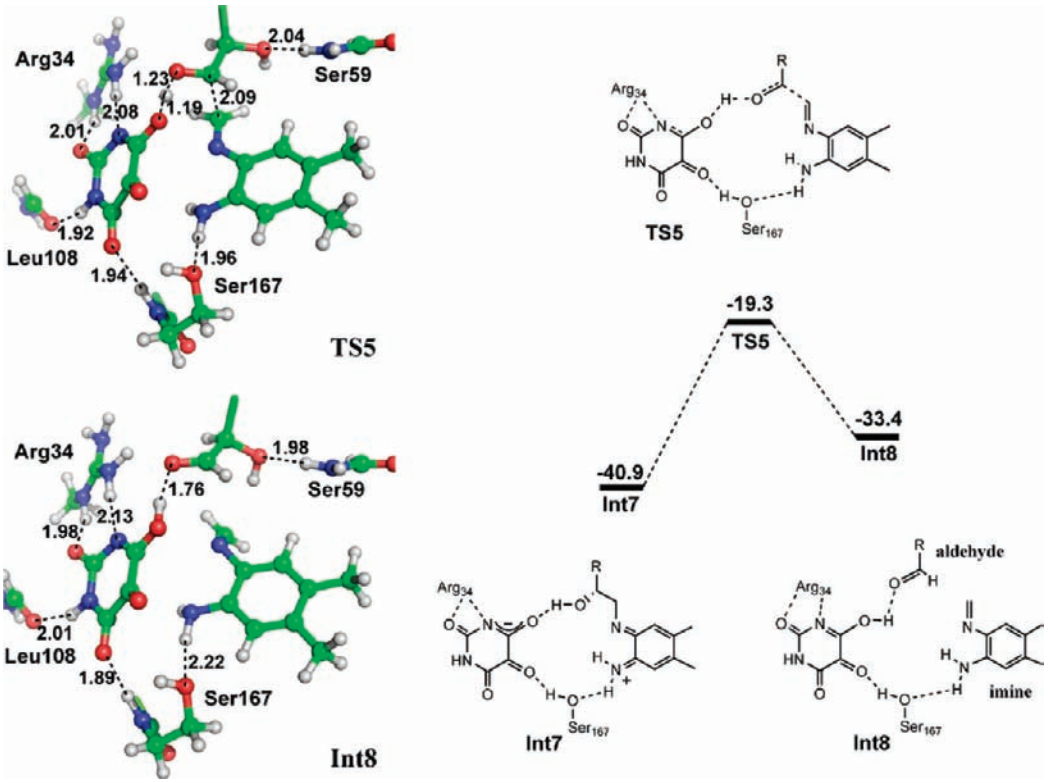

Figure 7. Optimized structures of transition state (**TS5**) and intermediate (**Int8**) of retro-aldol reaction. Some residues and fragments are omitted for clarity. Hydrogen bonds are shown by dashed lines, the distances are in angstroms, and energies are in kcal/mol.

negatively charged O10a of the deprotonated alloxan acts as a general base to abstract the proton from the hydroxyl on C2′ carbon, while the proton on N5 would stabilize the forming negative charge in the transition structure of the retro-aldol reaction. The transition structure is located at the C1′−C2′ bond distance of 2.09 Å, and the proton of the hydroxyl group on C2′ carbon is partially transferred to oxygen O10a of alloxan (Figure 7, **TS5**). The calculated activation barrier is 21.6 kcal/mol, which is the highest barrier along the suggested reaction path. These results are close to the experimental observation (k_{obs} = 3 min^{-1} ∼ 15 h^{-1}, corresponding to 19.2−20.7 kcal/mol),[18] but we notice this comparison should be made with considerable caution due to the expected error of about 3 kcal/mol for B3LYP method and the uncertainty of the exact dielectric constant in the protein environment.[58,59]

The retro-aldol reaction initiated from **Int4** or **Int6**, in which the proton is located on N1 or N10, respectively, was also investigated. The calculated activation barriers are more than 19 kcal/mol higher than that of **TS5** (Figure S6 and Figure S7), which suggests that the proton transfer from N1 of alloxan to N5 of the DMPDI fragment is required for the retro-aldol reaction.

Both Asp32 and Ser167 play crucial roles in the proton transfer process, in which Asp32 mediates the proton transfer from N1 to N5, while Ser167 stabilizes the protonated N5 and lowers the overall activation barrier. The stabilizing role of Ser167 is further confirmed by the testing calculations in which Ser167 is mutated to Gly167. **Int7** becomes about 4.3 kcal/mol less stable than **Int5** in S167G mutant, which raises the calculated barrier by about 1.5 kcal/mol compared to that for the wild type BluB (Figure S8). This result is consistent with experimental observation in which Ser167Gly mutant impedes the formation of DMB (about 30-fold less active).[18]

The retro-aldol cleavage between C1′ and C2′ carbons produces aldehyde and imine species. The produced aldehyde species is fully consistent with the experimental observation that D-erythrose 4-phosphate (E4P) rather than D-glyceraldehyde 3-phosphate (GA3P) is produced in the cannibalization of FMN catalyzed by BluB.[18] The imine species could be the ring-closing precursor to form DMB, which is consistent with the earlier observation that C2 of DMB is derived from C1′ of FMN. The conversion of the imine species to DMB is discussed in the following section.

3.5. Ring Closing and Formation of DMB. *3.5.1. Activation of the Imine.* The transformation of the imine species to DMB proceeds in three steps, including ring-closing step via the nucleophilic addition of the amino group to the carbon of the imine moiety, and the proton and hydride transfer from the ring-closing intermediate to the multifunctional alloxan to form DMB. However, direct ring closing from the neutral imine species has a high activation barrier of about 29.5 kcal/mol due to the low nucleophilicity of the aniline amino group and the low reactivity of the neutral imine group (Figure S9), highlighting that the activation of the imine group is necessary before the ring closing reaction.

The hydroxyl group (O10a−H) of alloxan is positioned well for activating the imine nitrogen N10. With the polarization of Arg34, the hydroxyl proton is readily transferred to the imine nitrogen N10 via a low activation barrier to break the hydrogen bond between the hydroxyl and the aldehyde (Figure 8, **TS6**). The produced intermediate (Figure 8, **Int9**) is stabilized by the hydrogen bonds between the deprotonated alloxan and the protonated imine, and also a nonclassical hydrogen bond between the protonated imine C−H and the negatively charged Asp32.

dx.doi.org/10.1021/ja1106207 |*J. Am. Chem. Soc.* 2011, 133, 4079–4091

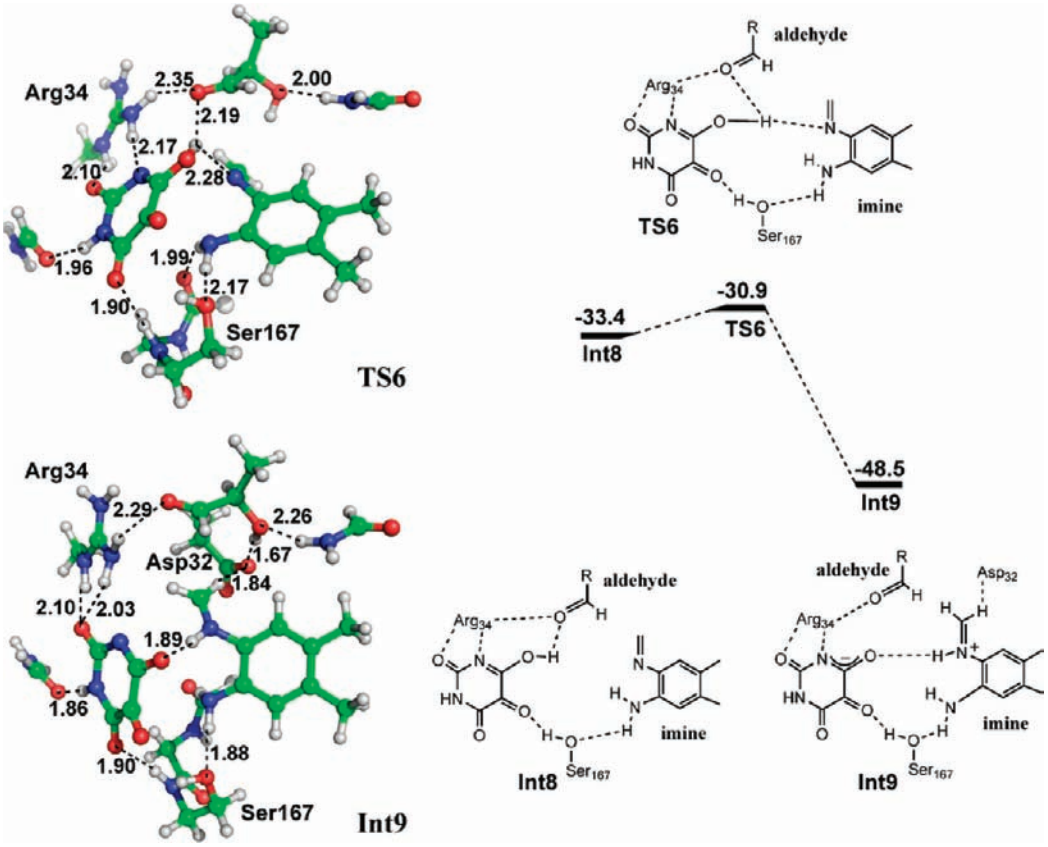

Figure 8. Energy profile and the optimized structures of transition state (**TS6**) and intermediate (**Int9**) of the proton transfer from alloxan to the imine species. Some residues and fragments are omitted for clarity. Hydrogen bonds are shown by dashed lines, the distances are in angstroms, and energies are in kcal/mol.

3.5.2. Ring Closing Reaction. The clockwise rotation of the imine group along the N10−C9a bond of **Int9** leads to the formation of the more stable intermediate **Int10** due to the stronger electrostatic interaction between the protonated imine and the more negatively charged Asp32. The transition from **Int9** to **Int10** is exothermic by 8.8 kcal/mol. The terminal carbon C1′ of the imine group in **Int10** is close to aniline N5 (2.99 Å), making it well positioned for the nucleophilic addition by N5 (Figure 9, **Int10**). The transition state of the nucleophilic addition of N5 to C1′ is located at the N5−C1′ distance of 2.19 Å (Figure 9, **TS7**), with an activation barrier of 12.3 kcal/mol, which is about 17 kcal/mol lower than that of the unactivated imine as described above (Figure S9). The positive charge is completely shifted from N10 to N5 in the subsequent intermediate **Int11**, and stabilized by Ser167 and the deprotonated alloxan. The newly formed 5,6-dimethyl-2,3-dihydro-1*H*-benzimidazole (H-DMB) in **Int11** is structurally close to DMB. However, to form the final product DMB, H-DMB requires loss of one hydride from C1′ and two protons from N10 and N5, respectively. This process will be discussed in the next subsection.

3.5.3. Formation of DMB. The requirement of losing hydride and protons for H-DMB to form DMB prompts us to look for the potential hydride and proton acceptors around H-DMB. In **Int11**, the three acidic protons of H-DMB form hydrogen bonds with the hydroxyl oxygen of Ser167, the oxygen O10a of the deprotonated alloxan, and the carboxylate oxygen of Asp32, respectively. Both the oxygen O10a of alloxan and the carboxylate oxygen of Asp32 carry negative charges, which makes them better proton acceptors than the hydroxyl oxygen of Ser167. On the other hand, alloxan has been reported as a good oxidizing agent for physiological reductants such as NAD(P)H and GSH.[60] Meanwhile, the predicted most active C4a[61] is also geometrically feasible for accepting a hydride from C1′ in **Int11**. Taken together, we propose the C4a carbon of alloxan as the possible hydride acceptor.

Though 5,6-dimethyl-2,3-dihydro-1*H*-benzimidazole (H-DMB) is a potential C−H hydride donor,[62] the protonated H-DMB is less likely to donate the hydride due to the formation of two nearby positive charges in the same species. Thus, the deprotonation of the positively charged N5 would occur prior to the hydride transfer. As shown in Figure 9, the hydrogen bond between the partially negatively charged oxygen O10a of the deprotonated alloxan and the protonated N5 facilitates the proton transfer from N5 to O10a to form the intermediate **Int12**. The proton transfer is slightly endothermic by 3.4 kcal/mol and with a calculated activation barrier of 15.2 kcal/mol (Figure 10 and Figure 11). That the proton located on O10a is less stable than that located on N5 can be explained by the polarization of the positively charged Arg34 on alloxan. On the other hand, the strongly acidic proton on O10a further polarizes the C4a−O4a carbonyl for the subsequent hydride transfer from C1′ to C4a, as reflected by the close distance between the C1′−H of H-DMB and C4a (2.20 Å) in **Int12**.

Once the proton is transferred from the protonated H-DMB to the deprotonated alloxan, the hydride transfer from C1′ of H-DMB to C4a of alloxan occurs readily with a low activation

dx.doi.org/10.1021/ja1106207 |*J. Am. Chem. Soc.* 2011, 133, 4079–4091

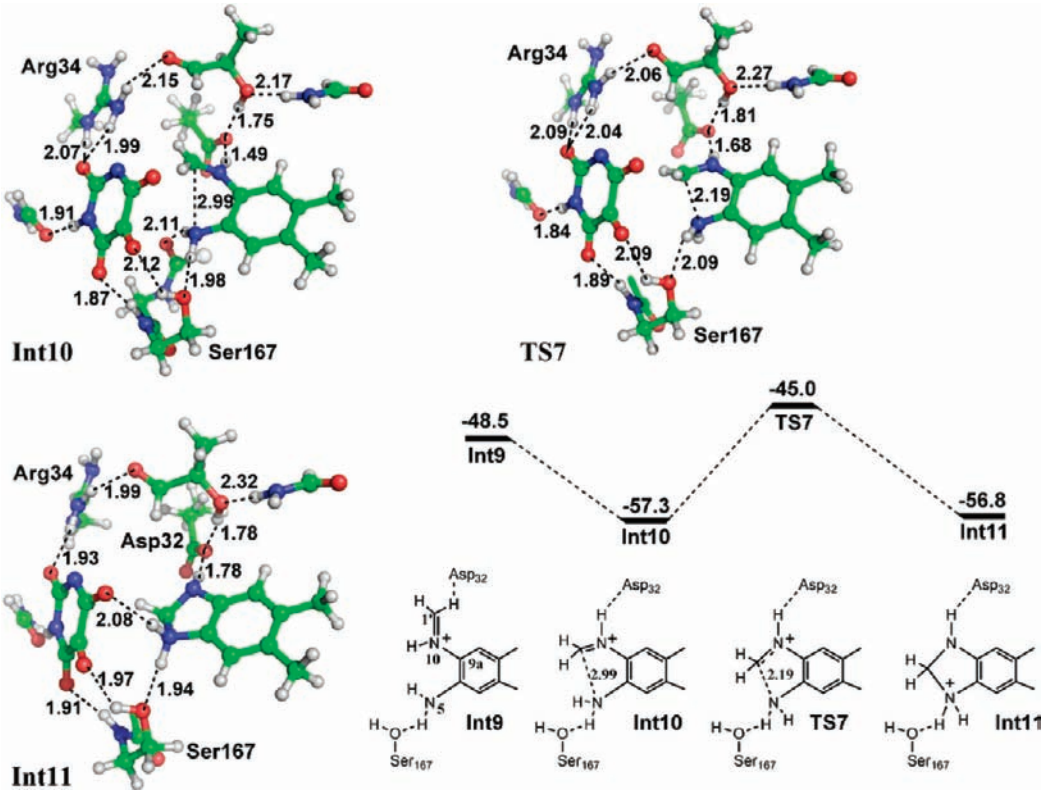

Figure 9. Optimized structures of the precursor (**Int10**), transition state (**TS7**), and product (**Int11**) of the ring closing reaction. Some residues and fragments are omitted for clarity. Hydrogen bonds are shown by dashed lines, the distances are in angstroms, and energies are in kcal/mol.

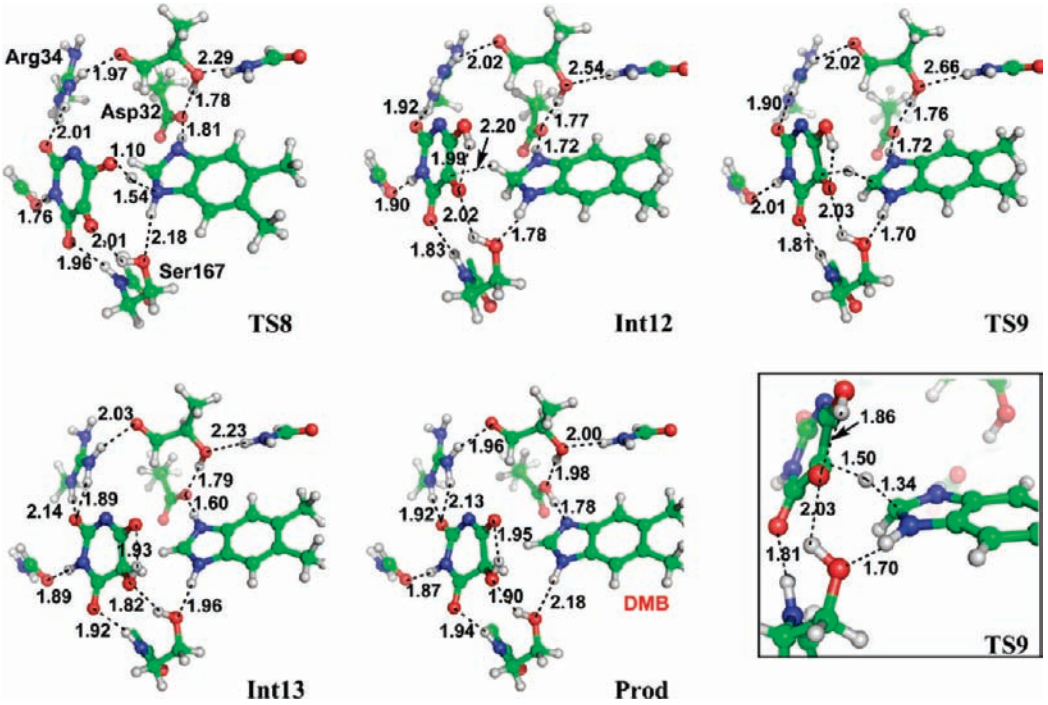

Figure 10. Optimized structures of the transition state (**TS8**) and intermediate (**Int12**) for the deprotonation of 5,6-dimethyl-2,3-dihydro-1*H*-benzimidazole, the transition state (**TS9**) and intermediate (**Int13**) for the hydride transfer from the 5,6-dimethyl-2,3-dihydro-benzimidazole to the alloxan, and the final formation of DMB (**Prod**). Some residues and fragments are omitted for clarity. Hydrogen bonds are shown by dashed lines, and the distances are in angstroms.

dx.doi.org/10.1021/ja1106207 |*J. Am. Chem. Soc.* 2011, 133, 4079–4091

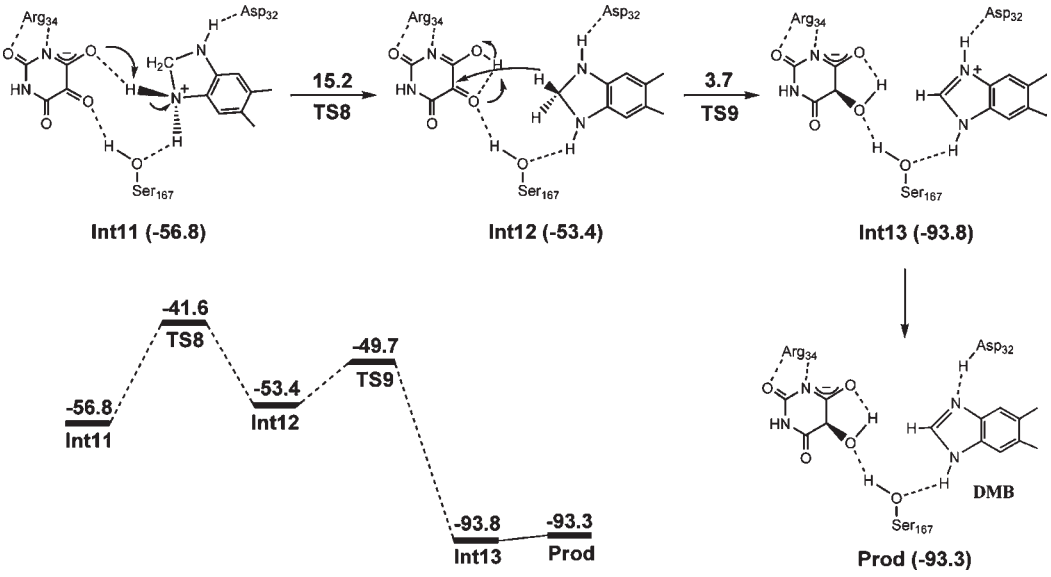

Figure 11. Schematic depiction of forming DMB from the intermediate 5,6-dimethyl-2,3-dihydro-1*H*-benzimidazole, and the potential energy profile. Energy is in kcal/mol.

barrier of 3.7 kcal/mol (Figure 11). The optimized structure of transition state for the hydride transfer (**TS9**) is shown in Figure 10, having the bond distances of C4a−H and C1′−H as 1.50 and 1.34 Å, respectively. This hydride transfer is in agreement with the stereochemical preference of removing *pro-R* hydrogen at C1′ of riboflavin in the previous experiment,[63] while in contrast to the stereochemical preference of the retention of *pro-R* hydrogen at C1′ in the nonenzymatic reactions,[22] which might highlight different mechanisms for the enzymatic and nonenzymatic reactions (see the Supporting Information for detailed discussions on the nonenzymatic reactions). The proton on O10a is transferred to O4a simultaneously with the hydride transfer to C4a, resulting in the formation of a dialuric acid (Figure 10, **Int13**). The formation of aromatic benzimidazolium cation in the intermediate **Int13** facilitates the proton transfer from N10 to the carboxylate oxygen of Asp32 to form the expected DMB (**Prod**).

As described above, the simple BluB can catalyze the complex transformation of $FMNH_2$ to DMB by consuming one oxygen molecule under the collaboration of the enzyme and intermediate. The formations of both E4P and DMB have been reasonably addressed in the proposed mechanism, while another calculated product, dialuric acid, still needs further identification and validation by the experiments. The previous experiments have shown that dialuric acid or its oxidized product alloxan could be metabolized to form urea by the microorganism,[64] and barbituric acid, analogue of dialuric acid, has been also shown to be metabolized to form urea by bacterial enzymes.[65,66] We therefore suggest that the reported urea from cell extracts[18,67] might be the metabolized product of dialuric acid or its oxidized form alloxan by as-yet-unidentified bacterial enzymes in cell extracts.

4. CONCLUSION

On the basis of the calculations, we propose a detailed mechanism for the conversion of FMN to DMB catalyzed by BluB, which involves multiple steps in two distinct stages (Scheme 2 and Figure 2). In the first stage, the dioxygen O_2 is first anchored and activated by the "oxygen hole" formed by the backbone amide of Gly61 and the O2′ hydroxyl group of $FMNH_2$; the conserved Asp32 then facilitates a single electron transfer from $FMNH_2$ to O_2 by partially deprotonating N1 of $FMNH_2$, which simultaneously activates both O_2 and $FMNH_2$ for the nucleophilic attack of O_2 to C4a to form the peroxyflavin intermediate. The subsequent formation and decomposition of the dioxetane-like intermediate lead to the fragmentation of $FMNH_2$ to form alloxan and DMPDI. In the second stage, BluB exploits alloxan as a multifunctional cofactor to catalyze the remaining steps of the reaction. First, alloxan sequentially serves as a proton donor and a proton acceptor to activate the ground state and stabilize the transition state of the retro-aldol cleavage of the C1′−C2′ bond of DMPDI to form E4P and the ring-closing precursor of DMB (**Int4** → **Int5** → **TS4** → **Int6** → **Int7** → **TS5** → **Int8**). Then, alloxan serves as a proton donor to activate the ring-closing precursor of DMB for the ring closing reaction, and sequentially serves as the proton and hydride acceptors to convert the ring-closing product to the final DMB (**Int8** → **TS6** → **Int9** → **Int10** → **TS7** → **Int11** → **TS8** → **Int12** → **TS9** → **Int13**).

The proposed mechanism for the conversion of $FMNH_2$ to DMB is consistent with the experiments in several aspects: (1) involvement of molecular oxygen in the reaction; (2) formation of E4P from the ribityl side chain by the cleavage of C1′−C2′ bond; (3) formation of DMB from the ring closing precursor in which C2 of DMB is derived from C1′ of $FMNH_2$; (4) the produced dialuric acid as the potential precursor of forming urea; (5) the catalytic roles of Asp32 and Ser167 in the reaction; (6) the calculated activation barrier of the rate-determining step with about 21 kcal/mol being close to the experimental observation, with the relatively slow catalysis of BluB possibly being necessary to avoid serious damage to the cell; (7) and more significantly, the suggested intermediate-assisted mechanism reasonably explaining how BluB with a relatively simple active site catalyzes such a complex conversion of $FMNH_2$ to DMB. In conclusion, the present studies provide significant insights into understanding the remarkable cannibalization of $FMNH_2$ to form DMB catalyzed by BluB. Meanwhile, the proposed mechanism

represents a new type of intermediate-assisted multifunctional catalysis in an enzymatic reaction, together with the substrate-assisted[68,69] and product-assisted[70] catalysis, which might also shed light on the evolution of enzymatic function in nature.

■ ASSOCIATED CONTENT

Supporting Information. Cartesian coordinates and calculated energies for all ground and transition structures. Energy profile and the optimized structures for Ser167Gly mutant in the retro-aldol reaction. Discussion on the nonenzymatic reactions. Complete ref 25. This material is available free of charge via the Internet at http://pubs.acs.org.

■ AUTHOR INFORMATION

Corresponding Author
quanjm@szpku.edu.cn

■ ACKNOWLEDGMENT

We are very grateful to Professors Yun-Dong Wu and Ya-Jun Liu for instructive discussion. We gratefully acknowledge financial support for this work from Peking University Shenzhen Graduate School, and the Shenzhen municipal "Shuang Bai Project".

■ REFERENCES

(1) Chui, C. H.; Lau, F. Y.; Wong, R.; Soo, O. Y.; Lam, C. K.; Lee, P. W.; Leung, H. K.; So, C. K.; Tsoi, W. C.; Tang, N.; Lam, W. K.; Cheng, G. *Nutrition* **2001**, *17*, 917–920.
(2) Ryan-Harshman, M.; Aldoori, W. *Can. Fam. Physician* **2008**, *54*, 536–541.
(3) Glusker, J. P. . In *Principles of Medical Biology: Molecular and Cellular Pharmacology*; Bittar, E. E., Bittar, N., Eds.; JAI Press Inc.: Greenwich, CT., 1997; Vol. 8C, pp 897−917.
(4) Jacobs, P.; Wood, L. *DM, Dis.-Mon.* **2003**, *49*, 636–645.
(5) Randaccio, L.; Geremia, S.; Wuerges, J. *J. Organomet. Chem.* **2007**, *692*, 1198–1215.
(6) Brown, K. L. *Chem. Rev.* **2005**, *105*, 2075–2149.
(7) Banerjee, R.; Ragsdale, S. W. *Annu. Rev. Biochem.* **2003**, *72*, 209–247.
(8) Banerjee, R. *Chem. Rev.* **2003**, *103*, 2083–2094.
(9) Toraya, T. *Chem. Rev.* **2003**, *103*, 2095–2127.
(10) Matthews, R. G. *Acc. Chem. Res.* **2001**, *34*, 681–689.
(11) Raux, E.; Schubert, H. L.; Warren, M. J. *Cell. Mol. Life Sci.* **2000**, *57*, 1880–1893.
(12) Roth, J. R.; Lawrence, J. G.; Bobik, T. A. *Annu. Rev. Biochem.* **1996**, *50*, 137–181.
(13) Scott, A. I. *J. Org. Chem.* **2003**, *68*, 2529–2539.
(14) Scott, A. I.; Roessner, C. A. *Pure Appl. Chem.* **2007**, *79*, 2179–2188.
(15) Campbell, G. R. O.; Taga, M. E.; Mistry, K.; Lloret, J.; Anderson, P. J.; Roth, J. R.; Walker, G. C. *Proc. Natl Acad. Sci. U.S.A.* **2006**, *103*, 4634–4639.
(16) Warren, M. J. *Proc. Natl Acad. Sci. U.S.A.* **2006**, *103*, 4799–4800.
(17) Gray, M. J.; Escalante-Semerena, J. C. *Proc. Natl Acad. Sci. U.S.A.* **2007**, *104*, 2921–2926.
(18) Taga, M. E.; Larsen, N. A.; Howard-Jones, A. R.; Walsh, C. T.; Walker, G. C. *Nature* **2007**, *446*, 449–453.
(19) Renz, P. *FEBS Lett.* **1970**, *6*, 187–189.
(20) Hörig, J. A.; Renz, P. *Eur. J. Biochem.* **1980**, *105*, 587–592.
(21) Renz, P.; Weyhenmeyer, R. *FEBS Lett.* **1972**, *22*, 124–126.
(22) Maggio-Hall, L. A.; Dorrestein, P. C.; Escalante-Semerena, J. C.; Begley, T. P. *Org. Lett.* **2003**, *5*, 2211–2213.
(23) Ealick, S. E.; Begley, T. P. *Nature* **2007**, *446*, 387–388.
(24) Begley, T. P.; Chatterjee, A.; Hanes, J. W.; Hazra, A.; Ealick, S. E. *Curr. Opin. Chem. Biol.* **2008**, *12*, 118–125.
(25) Frisch, M. J.; et al. *Gaussian 03, revision D.01*; Gaussian, Inc.: Wallingford CT, 2004 (see the Supporting Information for complete citation).
(26) Beck, A. D. *J. Chem. Phys.* **1993**, *98*, 5648–5652.
(27) Lee, C.; Yang, W.; Parr, R. G. *Phys. Rev. B* **1988**, *37*, 785–789.
(28) Siegbahn, P. E. M.; Blomberg, M. R. A. *Annu. Rev. Phys. Chem.* **1999**, *50*, 221–249.
(29) Siegbahn, P. E. M. *J. Biol. Inorg. Chem.* **2006**, *11*, 695–701.
(30) Siegbahn, P. E. M.; Borowski, T. *Acc. Chem. Res.* **2006**, *39*, 729–738.
(31) Bauschlicher, C. W., Jr.; Ricca, A.; Partridge, H.; Langhoff, S. R. . In *Recent Advances in Density Functional Methods, Part II*; Chong, D. P., Ed.; World Scientific Publishing Co.: Singapore, 1997; Vol. 1, pp 165−228.
(32) Isobe, H.; Yamanaka, S.; Kuramitsu, S.; Yamaguchi, K. *J. Am. Chem. Soc.* **2008**, *130*, 132–149.
(33) Barone, V.; Cossi, M. *J. Phys. Chem. A* **1998**, *102*, 1995–2001.
(34) Adamo, C.; Barone, V. *J. Chem. Phys.* **1999**, *110*, 6158–6170.
(35) Blomberg, M. R. A.; Siegbahn, P. E. M.; Babcock, G. T. *J. Am. Chem. Soc.* **1998**, *120*, 8812–8824.
(36) Harvey, J. N.; Aschi, M.; Schwarz, H.; Koch, W. *Theor. Chem. Acc.* **1998**, *99*, 95–99.
(37) Schmidt, M. W.; Baldridge, K. K.; Boatz, J. A.; Elbert, S. T.; Gordon, M. S.; Jensen, J. J.; Koseki, S.; Matsunaga, N.; Nguyen, K. A.; Su, S.; Windus, T. L.; Dupuis, M.; Montgomery, J. A. *J. Comput. Chem.* **1993**, *14*, 1347–1363.
(38) Fedorov, D. G.; Gordon, M. S. *J. Chem. Phys.* **2000**, *112*, 5611–5623.
(39) Nakamura, H. *J. Chem. Phys.* **1987**, *87*, 4031–4041.
(40) Malmstrom, B. G. *Annu. Rev. Biochem.* **1982**, *51*, 21–59.
(41) Massey, V. *J. Biol. Chem.* **1994**, *269*, 22459–22462.
(42) Prabhakar, R.; Siegbahn, P. E. M.; Minaev, B. F.; Ågren, H. *J. Phys. Chem. B* **2002**, *106*, 3742–3750.
(43) Minaev, B. F. *RIKEN Rev.* **2002**, *44*, 147–149.
(44) Kamerbeek, N. M.; Janssen, D. B.; Berkel, W. J. H.; Fraaije, M. W. *Adv. Synth. Catal.* **2003**, *345*, 667–678.
(45) Eswaramoorthy, S.; Bonanno, J. B.; Burley, S. K.; Swaminathan, S. *Proc. Natl Acad. Sci. U.S.A.* **2006**, *103*, 9832–9837.
(46) Berkel, W. J. H.; Kamerbeek, N. M.; Fraaije, M. W. *J. Biotechnol.* **2006**, *124*, 670–689.
(47) Sheng, D.-W.; Ballou, D. P.; Massey, V. *Biochemistry* **2001**, *40*, 11156–11167.
(48) Lei, B.-F.; Ding, Q.-Z.; Tu, S.-C. *Biochemistry* **2004**, *43*, 15975–15982.
(49) Campbell, Z. T.; Weichsel, A.; Montfort, W. R.; Baldwin, T. O. *Biochemistry* **2009**, *48*, 6085–6094.
(50) Macheroux, P.; Ghisla, S.; Hastings, J. W. *Biochemistry* **1993**, *32*, 14183–14186.
(51) Orlova, G.; Goddard, J. D.; Brovko, L. Y. *J. Am. Chem. Soc.* **2003**, *125*, 6962–6971.
(52) Chung, L. W.; Hayashi, S.; Lundberg, M.; Nakatsu, T.; Kato, H.; Morokuma, K. *J. Am. Chem. Soc.* **2008**, *130*, 12880–12881.
(53) Hirano, T.; Hasumi, Y.; Ohtsuka, K.; Maki, S.; Niwa, H.; Yamaji, M.; Hashizume, D. *J. Am. Chem. Soc.* **2009**, *131*, 2385–2396.
(54) Isobe, H.; Takano, Y.; Okumura, M.; Kuramitsu, S.; Yamaguchi, K. *J. Am. Chem. Soc.* **2005**, *127*, 8667–8679.
(55) Vico, L. D.; Liu, Y.-J.; Krogh, J. W.; Lindh, R. *J. Phys. Chem. A* **2007**, *111*, 8013–8019.
(56) Liu, F.-Y.; Liu, Y.-J.; Vico, L. D.; Lindh, R. *J. Am. Chem. Soc.* **2009**, *131*, 6181–6188.
(57) Wilsey, S.; Bernardi, F.; Olivucci, M.; Robb, M. A.; Murphy, S.; Adam, W. *J. Phys. Chem. A* **1999**, *103*, 1669–1677.
(58) Simonson, T.; Brooks, C. L., III. *J. Am. Chem. Soc.* **1996**, *118*, 8452–8458.

(59) Schutz, C. N.; Warshel, A. *Proteins: Struct., Funct., Genet.* **2001**, *44*, 400–417.
(60) Czerwińska, M.; Sikora, A.; Szajerski, P.; Adamus, J.; Marcinek, A.; Gębicki, J.; Bednarek, P. *J. Phys. Chem. A* **2006**, *110*, 7272–7278.
(61) Millefiori, S.; Millefiori, A. *J. Heterocycl. Chem.* **1987**, *24*, 525–527.
(62) Ryabukhin, S. V.; Plaskon, A. S.; Volochnyuk, D. M.; Shivanyuk, A. N.; Tolmachev, A. A. *J. Org. Chem.* **2007**, *72*, 7417–7419.
(63) Lingens, B.; Schild, T. A.; Vogler, B.; Renz, P. *Eur. J. Biochem.* **1992**, *207*, 981–985.
(64) Gray, C. T.; Brooke, M. S.; Gerhart, J. C. *J. Bacteriol.* **1961**, *81*, 755–761.
(65) Hayaishi, O.; Kornberg, A. *J. Biol. Chem.* **1952**, *197*, 717–732.
(66) Lara, F. J. S. *J. Bacteriol.* **1952**, *64*, 271–277.
(67) Renz, P. In *Chemistry and Biochemistry of B12*; Banerjee, R., Ed.; John Wiley & Sons: New York, 1999; pp 557−575.
(68) Dall'Acqua, W.; Carter, P. *Protein Sci.* **2000**, *9*, 1–9.
(69) Weinger, J. S.; Parnell, K. M.; Dorner, S.; Green, R.; Strobel, S. A. *Nat. Struct. Mol. Biol.* **2004**, *11*, 1101–1106.
(70) Fromme, J. C.; Bruner, S. D.; Yang, W.; Karplus, M.; Verdine, G. L. *Nat. Struct. Biol.* **2003**, *10*, 204–211.

NOTE ADDED AFTER ASAP PUBLICATION

Due to a production error equation 2 was incorrect in the version published ASAP February 23, 2011; the correct version reposted March 1, 2011.